

Nematic ordering of topological defects in active liquid crystals

Anand U. Oza¹ and Jörn Dunkel²

¹*Courant Institute of Mathematical Sciences, 251 Mercer Street, New York, NY 10012, USA*

²*Department of Mathematics, Massachusetts Institute of Technology,
77 Massachusetts Avenue, Cambridge, MA 02139-4307, USA*

(Dated: February 25, 2025)

Identifying the ordering principles of intracellular matter is key to understanding the physics of microbiological systems. Recent experiments show that ATP-driven microtubule-kinesin bundles can form non-equilibrium networks of liquid-crystalline order when trapped in an oil-water interface near a solid boundary. At high densities, the bundles realize a 2D active nematic phase characterized by spontaneous creation and annihilation of topological defects, reminiscent of particle-pair production processes in quantum systems. This remarkable discovery sparked considerable theoretical interest, yet a satisfactory mathematical description has remained elusive, primarily for the following two reasons. First, prevailing multi-component theories feature a large number of unknown parameters that make quantitative comparison with experiment infeasible. Second, the currently favored hydrodynamic models assume divergence-free 2D interfacial flow, thereby promoting turbulent pattern formation through upward cascades. Such cascades are unlikely to occur in experiments, where interface and bulk fluid can continuously exchange matter. Here, we propose a compact alternative continuum theory for dense active liquid crystals by merging ideas from the Landau-de Gennes and Swift-Hohenberg theories. The resulting fourth-order model agrees quantitatively with experimental data, correctly predicts a regime of long-range nematic alignment of defects, and manifests an analogy with a generalized Gross-Pitaevskii quantum theory. Generally, our results suggest that universal ordering principles may govern a wide range of active materials.

Active materials [1] assembled from intracellular components, such as DNA [2], microtubules and motor proteins [3, 4] promise innovative biotechnological applications, from microscale transport and medical devices [2] to artificial tissues [1] and programmable soft materials [5–7]. Beyond their practical value, these systems challenge theorists to generalize equilibrium statistical mechanics to far-from-equilibrium regimes [8–15]. Recent experimental advances in the self-assembly and manipulation of colloids with DNA-mediated interactions [16–18] have stimulated theoretical analysis that may eventually help clarify the physical principles underlying self-replication [19–21] and evolution in viruses [22–24] and other basic biological systems. Yet, despite some partial progress [9, 13, 14, 25, 26], our conceptual understanding of active materials remains far from complete. We do not know whether, or under which conditions, ‘universality’ ideas [27] that have proved powerful in the description of equilibrium systems can be generalized to describe collective dynamics of active matter. This deficit may be ascribed to the fact that in only very few instances mathematical models have been tested quantitatively against experiments [3, 28, 29].

An important class of non-equilibrium systems, which allows quantitative tests of universality concepts [27] and specific theories, are 2D active liquid crystal (ALC) analogs [4, 30–32]. ALCs are assemblies of rod-like particles that exhibit non-thermal collective excitations due to steady external [30, 31] or internal [4, 32] energy input. At high concentrations, ALCs form an active nematic phase characterized by dynamic creation and annihilation of topological defects [4, 30, 32], reminiscent of spontaneous particle-pair production in quantum systems.

This seemingly universal phenomenon was demonstrated recently [4, 32] for ATP-driven microtubule-kinesin bundles trapped in flat and curved oil-water interfaces. In the past two years, several multi-order-parameter models for this quintessential ALC system have been proposed [33, 34] but a large number of undetermined parameters is preventing systematic comparison with experiment. Whilst this drawback could in principle be overcome with more advanced computational resources in the future, there persist other more severe conceptual problems. Prevailing theories typically assume divergence-free 2D fluid flow within the interface which is unlikely to hold under realistic experimental conditions [4, 35]. As known for classical turbulence [36, 37], small-scale energy input can trigger turbulent upward cascades in incompressible 2D flow. Thus, topological defect dynamics in the current standard models may be dominated by an implausible incompressibility assumption, whereas in the experiments [4, 35] fluid can be exchanged continuously between interface and bulk (Fig. 1A). Another relevant yet previously ignored effect is damping from nearby solid boundaries, which can strongly influence the experimentally observed ALC dynamics [4, 35].

To overcome such limitations, we present here an alternative closed continuum theory for the nematic order-parameter tensor-field $Q(t, \mathbf{r})$ of dense ALCs. The proposed model generalizes recent higher-order scalar and vector theories of soft elastic materials [38] and bacterial fluids [28, 29] to matrix-valued fields. Our approach connects the classic Landau-de Gennes description of passive LCs [39] with the Swift-Hohenberg theory [40] of pattern formation and accounts explicitly for divergent interfacial flow and nearby boundaries. Imposing a Hele-Shaw-type

closure condition, we obtain an effective fourth-order partial differential equation (PDE) for Q . However, to resolve an unsatisfactory redundancy in the traditional description of dense 2D active nematics, we prefer an equivalent complex scalar field representation [41]. This representation reveals an otherwise hidden analogy with a generalized Gross-Pitaevskii theory [42, 43] of quantum gases, thereby establishing a direct mathematical link between ALCs and an important class of condensed matter systems. A systematic comparison with existing data confirms quantitative agreement between our theory and recent experiments [4, 35].

RESULTS

Theory. Previous multi-field models [33, 34] aim to describe the 2D nematic phase of a dense ALC suspension by coupling the filament concentration $c(t, \mathbf{r})$ and the nematic order tensor $Q(t, \mathbf{r})$ to an incompressible 2D flow field $\mathbf{v}(t, \mathbf{r})$ that satisfies $\nabla \cdot \mathbf{v} = 0$ in the interface plane $\mathbf{r} = (x, y)$. The nematic order parameter $S(t, \mathbf{r})$ is proportional to the larger eigenvalue of Q , and the filaments are oriented along the corresponding eigenvector, or director $\mathbf{d}(t, \mathbf{r})$. We here construct an alternative closed-form theory for the symmetric traceless 2×2 tensor field Q , starting from the generic transport law

$$\partial_t Q + \nabla \cdot (\mathbf{v}Q) - \alpha[Q, \omega] = -\frac{\delta \mathcal{F}}{\delta Q} \quad (1)$$

where $\omega = [\nabla \mathbf{v} - (\nabla \mathbf{v})^\top]/2$ is the vorticity tensor, $[A, B] = AB - BA$ the commutator of two matrices and $\mathcal{F}[Q] = \int d^2r F$ an effective free energy. Focussing on dense suspensions as realized in the experiments [4, 35], we neglect fluctuations in the microtubule concentration. It is important, however, that $\nabla \cdot (\mathbf{v}Q) \neq \mathbf{v} \cdot \nabla Q$ when $\nabla \cdot \mathbf{v} \neq 0$, which is typically the case when fluid can enter and leave the interface. Combining Landau-de Gennes theory [39] with Swift-Hohenberg theory [40], we postulate the free-energy density (SI Appendix)

$$F = \text{Tr} \left\{ -\frac{a}{2}Q^2 + \frac{b}{4}Q^4 - \frac{\gamma_2}{2}(\nabla Q)^2 + \frac{\gamma_4}{4}(\nabla \nabla Q)^2 \right\} \quad (2)$$

with $a, b > 0$ for the nematic phase. Assuming γ_2 can have either sign, ultraviolet stability requires $\gamma_4 > 0$. For $\gamma_2 < 0$, F possesses a homogeneous nematic ground-state manifold, whereas for $\gamma_2 > 0$ a pattern of characteristic wavelength $\Lambda \sim \sqrt{\gamma_4}/\gamma_2$ becomes energetically favorable, as shown below.

To obtain a closed Q -model, we relate the 2D flow field \mathbf{v} to Q through the linearly damped Stokes equation [44]

$$-\mu \nabla^2 \mathbf{v} + \nu \mathbf{v} = -\zeta \nabla \cdot Q \quad (3)$$

where μ is the viscosity and the rhs. represents active stresses [9, 33] with $\zeta > 0$ for extensile ALCs (Fig. 1B).

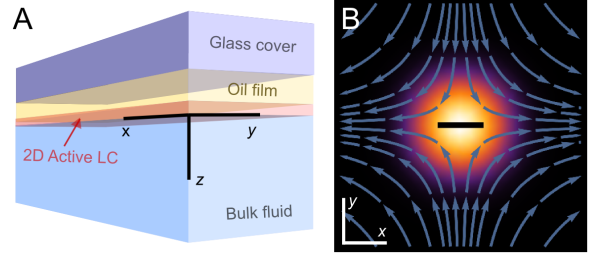


FIG. 1: (A) Schematic of the experimental setup reported in Ref. [4, 35], not drawn to scale. A thin oil film (thickness $\sim 3 \mu\text{m}$) separates a 2D ALC layer (2–10 nm) at the oil-water interface from a solid glass cover. Liquid can be exchanged between the ALC layer and bulk fluid, resulting in divergent 2D interfacial flow that is strongly damped by the nearby no-slip glass boundary and the viscous oil layer. (B) Extensile 2D dipole flow in the interface as predicted by the overdamped closure condition (4) for $D > 0$ and $Q = (\lambda, 0; 0, -\lambda)$ with $\lambda = \exp(-r^2)$. The central horizontal bar indicates the unit director axis, and background colors the nematic order parameter $S \sim \lambda$.

The ν -term in the force balance (3) accounts for friction from the nearby no-slip boundary in the Hele-Shaw [44] approximation (Fig. 1A). In the overdamped regime $\nu \Lambda^2/\mu \gg 1$, we deduce from Eq. (3) the closure condition

$$\mathbf{v} = -D \nabla \cdot Q, \quad D = \zeta/\nu. \quad (4)$$

Equation (4) predicts divergent interfacial flow, $\nabla \cdot \mathbf{v} \neq 0$, and hence fluid transport perpendicular to the interface wherever $\nabla \nabla : Q \neq 0$. Inserting (4) into (1) yields a closed Q -theory in which periodic director patterns corresponding to local minima of the free energy \mathcal{F} can become mixed by self-generated interfacial flow.

Complex representation. The traditional characterization of 2D nematic order in terms of the symmetric traceless 2×2 matrix field $Q = (\lambda, \mu; \mu, -\lambda)$ is redundant, for only two real scalar fields $\lambda(t, \mathbf{r})$ and $\mu(t, \mathbf{r})$ are needed to specify the nematic state at each position $\mathbf{r} = (x, y)$. To obtain an irreducible representation [41] we define the complex position coordinate $z = x + iy$, velocity field $\mathbf{v}(t, z) = u + iw$ and the complex order parameter $\psi(t, z) = \lambda + i\mu$, such that $S = 2|\psi|$. In terms of the Wirtinger gradient operator $\partial = \frac{1}{2}(\partial_x - i\partial_y)$, the 2D Laplacian takes the form $\nabla^2 = 4\bar{\partial}\partial$ and the closure condition (4) reduces to $v = -2D\bar{\partial}\psi$. Denoting the real and imaginary parts of an operator \mathcal{O} by $\Re\{\mathcal{O}\}$ and $\Im\{\mathcal{O}\}$, Eqs. (1) and (2) may be equivalently expressed as

$$\partial_t \psi + \mathcal{A}_\psi \psi = -\frac{\delta \mathcal{G}}{\delta \bar{\psi}} \quad (5)$$

where the self-advection operator is given by

$$\mathcal{A}_\psi = -4D \Re\{(\partial^2 \psi) + (\partial \psi) \partial\} + 4\alpha D i \Im\{\partial^2 \psi\} \quad (6)$$

and the free energy $\mathcal{G}[\psi, \bar{\psi}] = \int dz G$ has the density

$$G = -a|\psi|^2 + \frac{b}{2}|\psi|^4 + \gamma_2\bar{\psi}(4\bar{\partial}\partial)\psi + \gamma_4\bar{\psi}(4\bar{\partial}\partial)^2\psi. \quad (7)$$

For $\gamma_2 < 0$ and $\gamma_4 \rightarrow 0$, Eq. (7) reduces to the energy density of the Gross-Pitaevskii mean-field model [42, 43] for weakly interacting boson gases. This fact suggests an interesting connection between dense ALCs and quantum systems: when self-advection is negligible ($D \rightarrow 0$), the fixed point configurations of Eq. (5) coincide with the ‘eigenstates’ of generalized Gross-Pitaevskii models that incorporate wavelength selection.

Stability analysis. The qualitative model dynamics is not significantly altered for moderate values of α (Movies S1 and S2), so we neglect the commutator term by setting $\alpha = 0$ from now on (see SI Appendix for $\alpha > 0$). To understand the properties of Eqs. (5)–(6) when self-advection is relevant, we perform a fixed point analysis of the rescaled dimensionless equation (SI Appendix)

$$\partial_t\psi - 4D\Re\{(\partial^2\psi) + (\partial\psi)\partial\}\psi = \left(\frac{1}{4} - |\psi|^2\right)\psi - \gamma_2(4\bar{\partial}\partial)\psi - (4\bar{\partial}\partial)^2\psi, \quad (8)$$

by focussing on the uniform state $\psi_* = \frac{1}{2}e^{i2\theta}$, which corresponds to a nematic order parameter value $S = 1$ and homogeneous director angle θ relative to the x -axis. Considering wave-like perturbations $\psi = \psi_* + \hat{\epsilon}(t)e^{i\mathbf{k}\cdot\mathbf{r}}$ with $|\hat{\epsilon}| \ll 1$ and extensile ALCs with $D > 0$, one finds that ψ_* is generally unstable when $\gamma_2 > 0$ (SI Appendix). For subcritical self-advection, $D < D_c = 2(-\gamma_2 + \sqrt{\gamma_2^2 + 2})$, the most unstable mode $\mathbf{k}_* = k_*(\cos\phi_*, \sin\phi_*)$ is aligned parallel to the director, $(k_*, \phi_*) = (\sqrt{\gamma_2/(2\gamma_4)}, \theta)$, suggesting the formation of stripe patterns with typical wavelength $\Lambda \approx \sqrt{8\pi^2\gamma_4/\gamma_2}$. By contrast, for supercritical advection, $D > D_c$, the most unstable mode propagates perpendicular to the director, $(k_*, \phi_*) = (\sqrt{(2\gamma_2 + D)/(4\gamma_4)}, \theta + (\pi/2))$, suggesting the possibility of transverse mixing.

Phase diagram. To investigate the nonlinear dynamics of Eq. (8), we implemented a Fourier pseudospectral algorithm with modified Runge-Kutta time-stepping [45] (Methods) and so evolved the real and imaginary parts $\lambda(t, \mathbf{r})$ and $\mu(t, \mathbf{r})$ in time for periodic boundary conditions in space. A numerically obtained (γ_2, D) -phase diagram for random initial conditions confirms the existence of a turbulent nematic phase if active self-advection is sufficiently strong (Fig. 2A,B; Movie S1). Ordered configurations prevail at low activity (Fig. 2A,C,D; Movies S3, S4 and S5). Although the ground-states of the free energy (2) are in general not homogeneous, the critical curve separating the two regimes is in fair agreement with the estimate $D_c = 2(-\gamma_2 + \sqrt{\gamma_2^2 + 2})$ from linear stability of the homogenous state (black line in Fig. 2A). For subcritical values of the advection parameter D , we observe either defect-free ground-states or long-lived lattice-like states

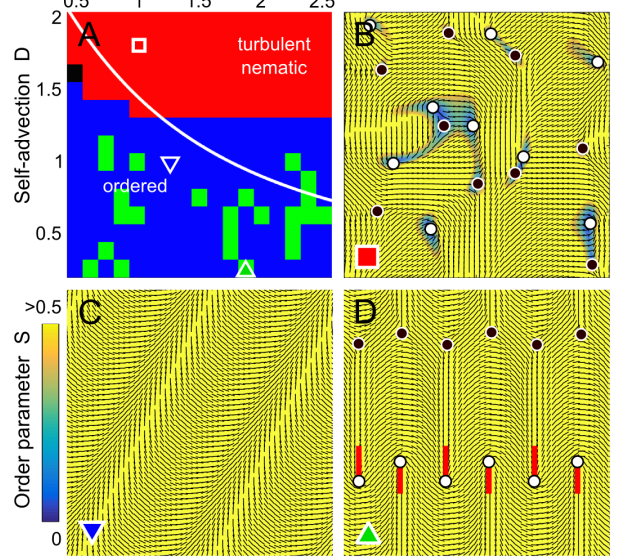


FIG. 2: Phase diagram obtained from simulations of Eq. (8) with random initial conditions showing the emergence of turbulent nematic states for supercritical active self-advection. (A) We observe convergence to defect-free stripes (blue, Panel C, Movie S3), time-periodic defect lattice solutions (green, Panel D, Movie S4), periodic defect creation and annihilation events (black, Movie S5), and chaotic dynamics (red, Panel B, Movie S1). The white line indicates the analytical estimate $D_c = 2(-\gamma_2 + \sqrt{\gamma_2^2 + 2})$ for the transitions between ordered and chaotic states. (B-D) Examples of the states identified in A with $-\frac{1}{2}$ -defects (black) and $+\frac{1}{2}$ -defects (white). Panel D highlights the antipolar nematic ordering of $+\frac{1}{2}$ -defect orientations (red bars).

exhibiting ordered defect configurations (Fig. 2C,D). Numerical free-energy calculations show that defect-free states (Fig. 2C) typically have slightly lower energies than the lattice states (Fig. 2D). Regarding the subsequent comparison of theory and experiment, it is important to note that the observed lattices generally exhibit antipolar nematic ordering of $+\frac{1}{2}$ -defects (Fig. 2D).

Theory vs. experiment. To test our theory systematically against existing experimental data [4, 35], we analyze defect-pair dynamics, global defect ordering and defect statistics in the turbulent nematic phase.

Spontaneous defect-pair creation and subsequent propagation, as reported in recent ALC experiments [4] and observed in our simulations, are compared in Fig. 3. In the experimental system [4], a $(+\frac{1}{2}, -\frac{1}{2})$ -defect pair is created when fracture along incipient crack regions [15] becomes energetically more favorable than buckling. After creation, the $+\frac{1}{2}$ -defect moves away rapidly whereas the position of the $-\frac{1}{2}$ -defect remains approximately fixed for up to several seconds (Fig. 3A). Our simulations of the minimal model defined in Eq. (8) accurately reproduce the details of the experimentally observed dynamics (Fig. 3B; Movies S1 and S2).

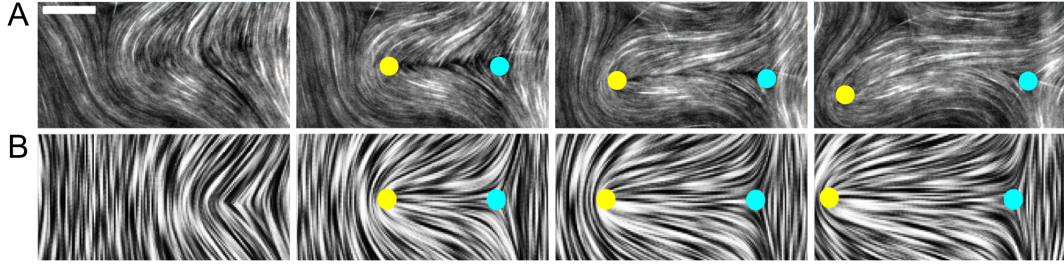


FIG. 3: Defect-pair creation and propagation in experiment and theory. (A) Experimentally observed dynamics of a defect pair, spontaneously produced by buckling and subsequent fracture of filaments; adapted with permission from Fig. 3d in Ref. [4]. Scale bar $20 \mu\text{m}$, time lapse 15 s. (B) Line integral convolution (LIC) plot of the director fields showing the spontaneous creation and propagation of a defect-pair in a simulation of Eq. (8) for $D = 1.5$, $\gamma_2 = 1$. As in the experiments, $+\frac{1}{2}$ -defects (yellow) generally move faster than $-\frac{1}{2}$ -defects (light blue), cf. Fig. 5.

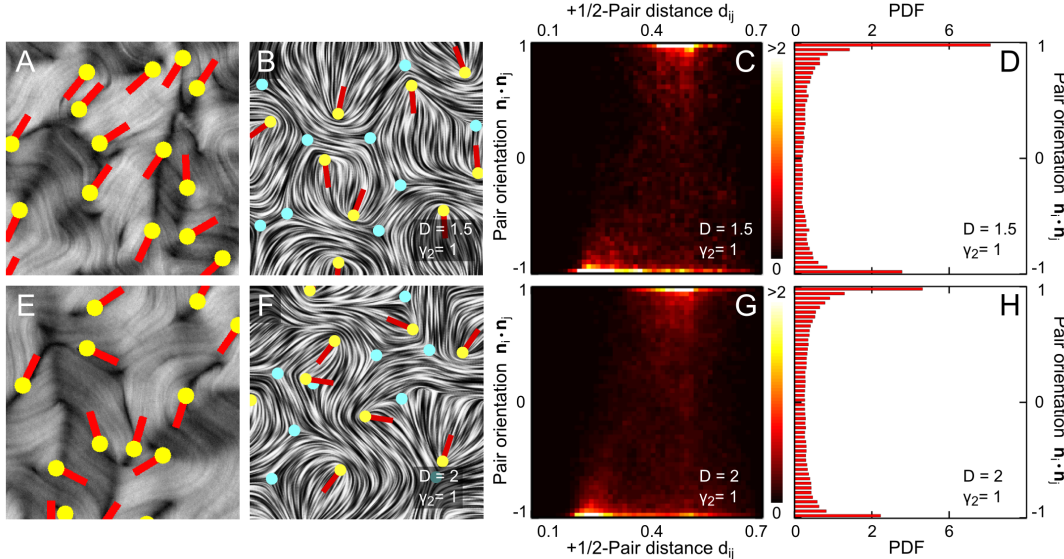


FIG. 4: Strong and weak nematic ordering of $+\frac{1}{2}$ -defects as (A,E) observed in experiments [35] and (B,F) predicted by our theory based on 2D simulations with periodic boundary conditions. Light-blue markers: $-\frac{1}{2}$ -defects. Yellow markers: $+\frac{1}{2}$ -defects. Red bars: orientation of $+\frac{1}{2}$ -defects. (A) $+\frac{1}{2}$ -defects in thin ALC films (thickness 2.1 nm) show strong global nematic alignment. (C,G) Maxima of the local pair orientation PDFs signal antipolar local ordering and nematic global ordering of $+\frac{1}{2}$ -defects, and reflect the typical defect-lattice spacing in units of the simulation box. (D,H) Global pair orientation distributions obtained by integrating the PDFs in (C,G) horizontally over all pair distances. (E) $+\frac{1}{2}$ -defects in thick ALC films (thickness 10.6 nm) show only weak local nematic alignment. (F-H) Increasing the effective hydrodynamic coupling D leads to stronger mixing and hence decreases nematic order. Figures A and E kindly provided by S. DeCamp and Z. Dogic.

Another striking and previously unexplained experimental observation [35] is the emergence of long-range nematic ordering of $+\frac{1}{2}$ -defect orientations in thin ALC layers (Fig. 4). Using the setup illustrated in Fig. 1A, recent experiments [35] demonstrated long-range nematic alignment of $+\frac{1}{2}$ -defects in thin ALC layers of thickness $h \sim 2.1 \text{ nm}$ (Fig. 4A), whereas thicker ALC layers with $h \sim 10.6 \text{ nm}$ showed no substantial orientational order on large scales (Fig. 4E). To investigate whether our theory can account for these phenomena, we tracked defect positions \mathbf{r}_i (Methods; Movie S1) and defect orientations $\mathbf{n}_i = \nabla \cdot \mathbf{Q}(\mathbf{r}_i) / |\nabla \cdot \mathbf{Q}(\mathbf{r}_i)|$ in sim-

ulations for different values of the advection parameter $D = \zeta/\nu$, since a Brinkmann-type scaling argument suggests that $1/\nu \sim h^2$. For weakly supercritical advection, $D \gtrsim D_c$, we find that Eq. (8) correctly predicts robust long-range nematic alignment of $+\frac{1}{2}$ -defects (Fig. 4B), as observed [35] in thin ALC layers (Fig. 4A). In our simulations, this ordering decreases as the effective mixing strength D increases (Fig. 4F), consistent with the experimental results [35] for thicker ALC layers (Fig. 4E). To quantify this effect, we recorded the distances d_{ij} between all $+\frac{1}{2}$ -defect pairs (i, j) as well as their relative orientations $\mathbf{n}_i \cdot \mathbf{n}_j \in [-1, 1]$. The re-

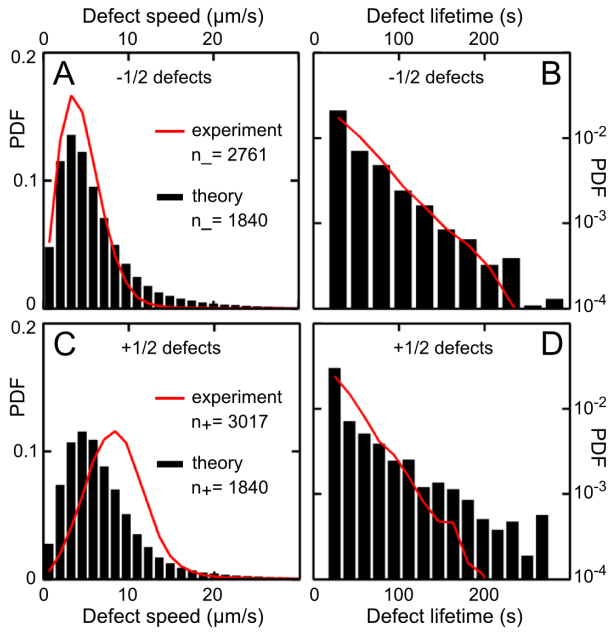


FIG. 5: Quantitative comparison of defect statistics between predictions of Eq. (8) and experimental data [35], using the parameter estimation procedure described in the text. For $-\frac{1}{2}$ -defects, both (A) speed distribution and (B) lifetime distribution agree well. (C) For $+\frac{1}{2}$ -defects, experimentally measured speed values are slightly larger, as our model assumes a strongly overdamped limit. (D) Simulations with periodic boundary conditions predict a low-probability tail of large lifetimes which is not visible in the experiment, likely due to its restricted field of view or additional noise. Dimensionless simulation parameters $D = 1.75$ and $\gamma_2 = 1$ translate into the following dimensional values: $a = 0.08 \text{ s}^{-1}$, $b = 0.33 \text{ s}^{-1}$, $D = 1641 \mu\text{m}^2/\text{s}$, $\gamma_2 = 937 \mu\text{m}^2/\text{s}$, $\gamma_4 = 2.66 \times 10^6 \mu\text{m}^4/\text{s}$. The numbers n_{\pm} reflect the number of $\pm\frac{1}{2}$ -defects tracked.

sulting local and global pair-orientation distributions for two different values of D are shown in Fig. 4C,D and G,H. The maxima at $\mathbf{n}_i \cdot \mathbf{n}_j = \pm 1$ in Fig. 4D,H signal global nematic alignment, whereas for polar ordering one would expect peaks only at $+1$. Moreover, the peak at $\mathbf{n}_i \cdot \mathbf{n}_j = -1$ for small distances indicates local antipolar ordering of nearby $+\frac{1}{2}$ -defects (Fig. 4C,G). A decrease in the maximum peak height for larger values of D indicates that enhanced hydrodynamic mixing reduces nematic ordering (Fig. 4D,H).

Lastly, we test the theoretically predicted defect statistics against an experimental data set kindly provided by DeCamp *et al.* [35]. Since our simulations are performed in dimensionless units, there is freedom to choose a characteristic lengthscale l_0 and timescale t_0 . To relate theory and experiments, we determine (l_0, t_0) such that the joint mean speed and mean lifetime of $\pm\frac{1}{2}$ -defects match the experimental values $\bar{v} = 6.6 \mu\text{m/s}$ and $\bar{\tau} = 52.8 \text{ s}$. After fixing these global scales, we can compare details of the speed and lifetime distributions (Fig. 5). To this end, we first locate the ‘best-fit’ simulation parameters

in the (γ_2, D) -grid space explored in the phase diagram (Fig. 2). This procedure identifies $\gamma_2 = 1, D = 1.75$ as the best-match parameters although nearby parameter values and simulations with $\alpha = 1$ produce fits of similar quality, corroborating the robustness of the model (Fig. S3). For $-\frac{1}{2}$ -defects, we find adequate agreement between experiment and theory for speed and lifetime probability density functions (PDFs), as evident from Fig. 5A,B. For $+\frac{1}{2}$ -defects, simulation results also agree well with the experimental measurements (Fig. 5C,D), but one notices two systematic differences. First, while the peak heights of the PDFs agree within a few percent, experimentally measured speed values for $+\frac{1}{2}$ -defects are on average slightly larger than theoretically predicted values (Fig. 5C). Second, simulation data predict a minuscule tail-fraction of long-living $+\frac{1}{2}$ -defects not detected in the experiment (Fig. 5D). In addition, based on the experimental density estimate of 30 defects/mm² [35], we find that the total number of defects at any given time in the ‘best-fit’ simulation is $\sim 2.1 \times$ lower than in the experiments. As discussed below, such deviations can be explained plausibly by specific model assumptions. Taken together, the above results confirm that the minimal model defined by Eq. (8) provides a satisfactory qualitative and quantitative description of the main experimental results [4, 35].

DISCUSSION

Universality. Equations (2) and (7) epitomize the idea of ‘universality’ in spatio-temporal pattern formation [40, 46]. More precisely, the free-energy expressions contain the leading-order terms of generic series expansions in both order-parameter space and Fourier space. When considering passive systems with a preference for homogenization ($\gamma_2 < 0$), it usually suffices to keep only the quadratic gradient terms. By contrast, for pattern forming systems, the coefficient in front of the lowest-order gradient contribution can change sign [38, 40], and one must include higher-order derivatives to ensure stability. In a few select cases, expressions of the form (2) and (7) can be systematically derived [38, 40, 47]. Generally, one can regard the free-energy expansion (7) as an effective field theory whose phenomenological parameters can be determined from experiments. This approach has proved successful for dense bacterial suspensions [28, 29] and now also for ALCs, indeed suggesting some universality in the formation and dynamics of topological defects in active systems.

Nematic defect order. Although (γ_2, D) are varied as independent effective parameters in the simulations, they are likely coupled through underlying physical and chemical parameters. For example, it is plausible that a change in ATP-concentration or film-thickness would affect both γ_2 and D . The parameter D can also be interpreted as an effective Reynolds number. In our numerical exploration of the (γ_2, D) -parameter space, we ob-

serve for subcritical advection D either long-lived lattice-like states exhibiting nematically aligned $+\frac{1}{2}$ -defects or defect-free ground-states (Fig. 2; Movies S3, S4 and S5). Ordered defect configurations correspond to local minima or saddles in the free-energy landscape and have only slightly higher energy than defect-free states (Fig. 2C). When the activity ζ is sufficiently large that advection is marginally supercritical, $D \gtrsim D_c$, chaotic system trajectories spend a considerable time in the vicinity of these metastable lattice states (Movies S1), which explains the experimentally observed ordering of defects in thin ALC films [35]. For $D \gg D_c$, the ALC system can access a wider range of high-energy states, leading to increased disorder in the defect dynamics. Although the strongly turbulent regime $D \gg D_c$ is difficult to realize with our current simulation code, the reduction in nematic defect order at larger values of D is evident from the reduced peak height in Fig. 4H relative to Fig. 4D.

Defect statistics. The systematic speed deficit in Fig. 5C reflects the overdamped closure condition (4), which suppresses the propagation of hydrodynamic excitations. Since flow in a newly created defect pair generally points from the $-\frac{1}{2}$ to the $+\frac{1}{2}$ -defect, the minimal model (8) can be expected to underestimate the speeds of $+\frac{1}{2}$ -defects. This effect could be explored in future experiments through a controlled variation of the thickness and viscosity of the oil film (Fig. 1A). The low-probability tail of long-living $+\frac{1}{2}$ -defects in the simulation data (Fig. 5D) may be due to the fact that defects can be tracked indefinitely in the simulations. By contrast, long-living $+\frac{1}{2}$ -defects are likely to leave the finite field of view in the experiments. In the future, our minimal theory can be extended systematically by adding terms to the free-energy or by explicitly simulating the full hydrodynamics in Eq. (3). Such extensions will likely improve further the quantitative agreement between experiment and theory.

CONCLUSIONS

Recent experimental and theoretical studies showed that fourth-order PDE models for scalar and vector fields provide an accurate quantitative description of surface-pattern formation in soft elastic materials [38]

and orientational order in dense bacterial fluids [28, 29]. Here, we have generalized these ideas to matrix-valued fields describing soft active nematics. The above analysis demonstrates that a generic fourth-order Q -tensor model can account for previously unexplained experimental observations in 2D ALCs [35], including the emergence of long-range nematic ordering of topological defects. The fact that three vastly different soft matter systems can be treated quantitatively in terms of structurally similar higher-order PDEs [28, 29, 38] promises a unified mathematical framework for the description of pattern formation processes in a broad class of complex materials. In addition, the free-energy analogy [41] between dense ALCs and generalized Gross-Pitaevskii models suggests that the self-organization principles [27] of mesoscopic active matter and microscopic quantum systems could be more similar than previously thought.

Acknowledgments. This work was supported by the NSF Mathematical Sciences Postdoctoral Research Fellowship DMS-1400934 (A.O.), an MIT Solomon Buchsbaum Award (J.D.) and an Alfred P. Sloan Research Fellowship (J.D.). The authors would like to thank Zvonimir Dogic and Stephen DeCamp for kindly sharing their experimental data, and Michael Hagan, Ken Kamrin, Mehran Kardar, Jontasz Slomka, Norbert Stoop and Francis Woodhouse for insightful discussions.

METHODS

Numerical solver & defect tracking. To simulate Eq. (8), we implemented a numerical algorithm that evolves the real and imaginary parts $\lambda(t, \mathbf{r})$ and $\mu(t, \mathbf{r})$ in time for periodic boundary conditions in space. The algorithm solves Eq. (8) pseudospectrally in space with ≥ 256 lattice points in each direction, and steps forward in time using a modified exponential time-differencing fourth-order Runge-Kutta method [45] with time step $\Delta t = 2^{-10}$. Simulations were initialized with either a single defect pair or random field configurations $\{\lambda(0, \mathbf{r}), \mu(0, \mathbf{r})\}$. Defects are located at the intersections of the zero-contours of λ and μ , and we tracked their positions by implementing James Munkres' variant of the Hungarian assignment algorithm [48] (SI Appendix).

[1] M. A. McEvoy and N. Correll. Materials that couple sensing, actuation, computation, and communication. *Science*, 347(6228), 2015.

[2] S. M. Douglas, A. H. Marblestone, S. Teerapittayanon, A. Vazquez, G. M. Church, and W. M. Shih. Rapid prototyping of 3D DNA-origami shapes with caDNAno. *Nucl. Acids Res.*, 37(15):5001–5006, 2009.

[3] V. Schaller, C. Weber, C. Semmrich, E. Frey, and A. R. Bausch. Polar patterns of driven filaments. *Nature*, 467:73–77, 2010.

[4] T. Sanchez, D. T. N. Chen, S. J. DeCamp, M. Heymann, and Z. Dogic. Spontaneous motion in hierarchically assembled active matter. *Nature*, 491:431, 2012.

[5] P. W. K. Rothemund. Folding DNA to create nanoscale shapes and patterns. *Nature*, 440(7082):297–302, 03 2006.

[6] P. C. Nickels, Y. Ke, R. Jungmann, D. M. Smith, M. Leichsenring, W. M. Shih, T. Liedl, and B. Högberg. DNA Origami Structures Directly Assembled from Intact Bacteriophages. *Small*, 10(9):1765–1769, 2014.

[7] A. R. Studart and R. M. Erb. Bioinspired materials that self-shape through programmed microstructures. *Soft Matter*, 10:1284–1294, 2014.

[8] J. Toner and Y. Tu. Flocks, herds, and schools: A quantitative theory of flocking. *Phys. Rev. E*, 58(4):4828–4858, 1998.

[9] R. A. Simha and S. Ramaswamy. Hydrodynamic fluctuations and instabilities in ordered suspensions of self-propelled particles. *Phys. Rev. Lett.*, 89(5):058101, 2002.

[10] D. Saintillan and M. Shelley. Instabilities, pattern formation and mixing in active suspensions. *Phys. Fluids*, 20:123304, 2008.

[11] L. Giomi, L. Mahadevan, B. Chakraborty, and M. F. Hagan. Excitable patterns in active nematics. *Phys. Rev. Lett.*, 106:218101, 2011.

[12] M. Ravnik and J. M. Yeomans. Confined active nematic flow in cylindrical capillaries. *Phys. Rev. Lett.*, 110:026001, 2013.

[13] T. C. Adhyapak, S. Ramaswamy, and J. Toner. Live soap: Stability, order, and fluctuations in apolar active smectics. *Phys. Rev. Lett.*, 110:118102, 2013.

[14] M. C. Marchetti, J. F. Joanny, S. Ramaswamy, T. B. Liverpool, J. Prost, M. Rao, and R. A. Simha. Hydrodynamics of soft active matter. *Rev. Mod. Phys.*, 85:1143, 2013.

[15] T. Gao, R. Blackwell, M. A. Glaser, M. D. Betterton, and M. J. Shelley. Multiscale polar theory of microtubule and motor-protein assemblies. *Phys. Rev. Lett.*, 114:048101, 2015.

[16] C. A. Mirkin, R. L. Letsinger, R. C. Mucic, and J. J. Storhoff. A DNA-based method for rationally assembling nanoparticles into macroscopic materials. *Nature*, 382(6592):607–609, 1996.

[17] M.-P. Valignat, O. Theodoly, J. C. Crocker, W. B. Russel, and P. M. Chaikin. Reversible self-assembly and directed assembly of DNA-linked micrometer-sized colloids. *Proc. Natl. Acad. Sci. U.S.A.*, 102(12):4225–4229, 2005.

[18] J. Palacci, S. Sacanna, A. P. Steinberg, D. J. Pine, and P. M. Chaikin. Living crystals of light-activated colloidal surfers. *Science*, 339(6122):936–940, 2013.

[19] W. Ebeling, A. Engel, and R. Feistel. *Physik der Evolutionsprozesse*. Akademie Verlag, 1992.

[20] Z. Zeravcic and M. P. Brenner. Self replicating colloidal clusters. *Proc. Natl. Acad. Sci. U.S.A.*, 111(5):1748–1753, 2014.

[21] J. L. England. Statistical physics of self-replication. *J. Chem. Phys.*, 139:121923, 2013.

[22] B. Berger, P. W. Shor, L. Tucker-Kellogg, and J. King. Local rule-based theory of virus shell assembly. *Proc. Natl. Acad. Sci. U.S.A.*, 91(16):7732–7736, 1994.

[23] J. D. Perlmutter and M. F. Hagan. Mechanisms of virus assembly. *Annu. Rev. Phys. Chem.*, 66:217–239, 2015.

[24] G. Meng, J. Paulose, D. R. Nelson, and V. N. Manoharan. Elastic instability of a crystal growing on a curved surface. *Science*, 343(6171):634–637, 2014.

[25] T. Vicsek and A. Zafeiris. Collective motion. *Physics Reports*, 517(3-4):71–140, 2012.

[26] S. Ramaswamy. The mechanics and statistics of active matter. *Annu. Rev. Cond. Mat. Phys.*, 1:323–345, 2010.

[27] N. Goldenfeld and C. Woese. Life is physics: Evolution as a collective phenomenon far from equilibrium. *Annual Rev. Cond. Mat. Phys.*, 2(1):375–399, 2011.

[28] H. H. Wensink, J. Dunkel, S. Heidenreich, K. Drescher, R. E. Goldstein, H. Löwen, and J. M. Yeomans. Mesoscale turbulence in living fluids. *Proc. Natl. Acad. Sci. USA*, 109(36):14308–14313, 2012.

[29] J. Dunkel, S. Heidenreich, K. Drescher, H. H. Wensink, M. Bär, and R. E. Goldstein. Fluid dynamics of bacterial turbulence. *Phys. Rev. Lett.*, 110:228102, 2013.

[30] V. Narayan, S. Ramaswamy, and N. Menon. Long-lived giant number fluctuations in a swarming granular nematic. *Science*, 317:105–108, 2007.

[31] I. S. Aranson, A. Snezhko, J. S. Olafsen, and J. S. Urbach. Comment on "Long-Lived Giant Number Fluctuations in a Swarming Granular Nematic". *Science*, 320(5876):612, 2008.

[32] F. C. Keber, E. Loiseau, T. Sanchez, S. J. DeCamp, L. Giomi, M. J. Bowick, M. C. Marchetti, Z. Dogic, and A. R. Bausch. Topology and dynamics of active nematic vesicles. *Science*, 345(6201):1135–1139, 2014.

[33] S. P. Thampi, R. Golestanian, and J. M. Yeomans. Velocity correlations in an active nematic. *Phys. Rev. Lett.*, 111:118101, 2013.

[34] L. Giomi, M. J. Bowick, X. Ma, and M. C. Marchetti. Defect annihilation and proliferation in active nematics. *Phys. Rev. Lett.*, 110:228101, 2013.

[35] S. J. DeCamp, G. S. Redner, A. Baskaran, M. F. Hagan, and Z. Dogic. Orientational order of motile defects in active nematics. arXiv:1501.06228v2, 2015.

[36] R. H. Kraichnan and D. Montgomery. Two-dimensional turbulence. *Rep. Prog. Phys.*, 43:547–619, 1980.

[37] H. Kellay and W. I. Goldburg. Two-dimensional turbulence: a review of some recent experiments. *Rep. Prog. Phys.*, 65:845–894, 2002.

[38] N. Stoop, R. Lagrange, D. Terwagne, P. M. Reis, and J. Dunkel. Curvature-induced symmetry breaking determines elastic surface patterns. *Nature Materials*, 14:337–342, 2015.

[39] P. G. de Gennes and J. Prost. *The Physics of Liquid Crystals*, volume 2. Oxford University Press, Oxford, 1995.

[40] J. Swift and P. C. Hohenberg. Hydrodynamic fluctuations at the convective instability. *Phys. Rev. A*, 15(1):319–328, 1977.

[41] S. R. Renn and T. C. Lubensky. Abrikosov dislocation lattice in a model of the cholesteric-to-smectic-*A* transition. *Phys. Rev. A*, 38:2132–2147, Aug 1988.

[42] E. P. Gross. Structure of a quantized vortex in boson systems. *Nuovo Cim.*, 20(3):454–477, 1961.

[43] L. P. Pitaevskii. Vortex lines in an imperfect Bose gas. *Sov. Phys. JETP*, 13(2):451–454, 1961.

[44] F. G. Woodhouse and R. E. Goldstein. Cytoplasmic streaming in plant cells emerges naturally by microfilament self-organization. *Proc. Natl. Acad. Sci. U.S.A.*, 110(35):14132–14137, 2013.

[45] A.-K. Kassam and L. N. Trefethen. Fourth-order time-stepping for stiff PDEs. *SIAM J. Sci. Comput.*, 26(4):1214–1233, 2005.

[46] I. S. Aranson and L. S. Tsimring. Patterns and collective behavior in granular media: Theoretical concepts. *Rev. Mod. Phys.*, 78:641–692, 2006.

[47] R. Großmann, P. Romanczuk, M. Bär, and L. Schimansky-Geier. Vortex arrays and mesoscale turbulence of self-propelled particles. *Phys. Rev. Lett.*, 113:258104, 2014.

[48] J. Munkres. Algorithms for assignment and transportation problems. *J. Soc. Indust. Appl. Math.*, 5(1):32–38, 1957.